SO(5) symmetry in the quantum Hall effect in graphene

Fengcheng Wu,[1] Inti Sodemann,[1,*] Yasufumi Araki,[1] Allan H. MacDonald,[1,†] and Thierry Jolicoeur[2,‡]
[1]*Department of Physics, University of Texas at Austin, Austin, Texas 78712, USA*
[2]*Laboratoire de Physique Théorique et Modèles statistiques, CNRS and Université Paris-Sud, Orsay 91405, France*
(Received 3 August 2014; revised manuscript received 8 December 2014; published 22 December 2014)

Electrons in graphene have four flavors associated with low-energy spin and valley degrees of freedom. The fractional quantum Hall effect in graphene is dominated by long-range Coulomb interactions, which are invariant under rotations in spin-valley space. This SU(4) symmetry is spontaneously broken at most filling factors, and also weakly broken by atomic scale valley-dependent and valley-exchange interactions with coupling constants g_z and $g_\perp$. In this paper, we demonstrate that when $g_z = -g_\perp$, an exact SO(5) symmetry survives which unifies the Néel spin order parameter of the antiferromagnetic state and the XY valley order parameter of the Kekulé distortion state into a single five-component order parameter. The proximity of the highly insulating quantum Hall state observed in graphene at $\nu = 0$ to an ideal SO(5) symmetric quantum Hall state remains an open experimental question. We illustrate the physics associated with this SO(5) symmetry by studying the multiplet structure and collective dynamics of filling factor $\nu = 0$ quantum Hall states based on exact-diagonalization and low-energy effective theory approaches. This allows to illustrate how manifestations of the SO(5) symmetry would survive even when it is weakly broken.

DOI: 10.1103/PhysRevB.90.235432 PACS number(s): 73.22.Pr, 73.43.−f

I. INTRODUCTION

Electron-electron interactions in the fractional quantum Hall effect (FQHE) regime give rise to a host of nonperturbative and unexpected phenomena, including importantly the emergence of quasiparticles with fractional charge and statistics. In this paper, we suggest that neutral graphene in the FQHE regime could also provide a relatively simple example of the complex many-particle physics that occurs in systems with simultaneous quantum fluctuations of competing order parameters. Because each of its Landau levels has a fourfold spin/valley flavor degeneracy in the absence of Zeeman coupling, large gaps and associated quantum Hall effects are produced by single-particle physics only at filling factors $\nu = \pm 2, \pm 6, \ldots$. The quantum Hall effect nevertheless occurs at all intermediate integer filling factors [1,2], and at many fractional filling factors [3–5], usually [6] with a broken symmetry incompressible ground state. When lattice corrections to the continuum Dirac model's Coulomb interactions are ignored, the ground state at neutrality ($\nu = 0$) is a Slater determinant [7] with all the $N = 0$ single-particle states of two arbitrarily chosen flavors occupied and, because the Hamiltonian is SU(4) invariant, it has four independent degenerate Goldstone modes. The rich flavor physics of graphene in the quantum Hall regime has already been established by experiments that demonstrate that phase transitions between distinct many-electron states with the same filling factor ν can be driven by tuning the magnetic field strength or the tilt angle [8–12].

In graphene, the competition between states with Kekulé-distorion (KD), antiferromagnetic (AF), ferromagnetic (F), charge-density wave (CDW), and other types of order is controlled by Zeeman coupling to the electron spin, and also by weak atomic-range valley-dependent [13] interactions. A variety of approaches have been used to estimate these short-range corrections to the Coulomb interaction [14–20]. In this paper, we adopt a two-parameter phenomenological model motivated by crystal momentum conservation and by the expectation that corrections to the Coulomb interaction are significant only at distances shorter than a magnetic length [20] $l_B = \sqrt{\hbar c/eB_\perp}$. ($B_\perp$ is the magnetic field component perpendicular to the graphene plane.) We demonstrate that along a line in this parameter space SU(4) symmetry is reduced only to a SO(5) subgroup. In this paper, we take interaction-driven quantum Hall states at $\nu = 0$ as an example to illustrate the physical manifestation of the SO(5) symmetry. We explicitly derive a low-energy theory at $\nu = 0$ that is able to account simultaneously for Néel antiferromagnetism and Kekulé lattice-distortion order and demonstrate that along the SO(5) line the four collective modes remain gapless in spite of the reduced symmetry. The exact SO(5) symmetry we have identified in graphene's quantum Hall regime is analogous to the approximate symmetry conjectured in some models of high-T_c superconductivity [21]. Our work demonstrates that an enlarged symmetry like SO(5) can indeed be exactly realized in a realistic microscopic Hamiltonian. In the following, we start with a systematic analysis of Hamiltonian symmetries and then use both exact-diagonalization and low-energy effective models at $\nu = 0$ to identify some symmetry-related properties.

Although our work focuses on the properties of the quantum Hall state at neutrality, we demonstrate that the SO(5) symmetry is an exact symmetry of the interaction Hamiltonian for the quantum Hall states in the zero-energy Landau level of graphene. Therefore this symmetry is expected to emerge as well in the phase diagrams at arbitrary filling fractions in this Landau level.

The quantum Hall state of graphene at neutrality is believed to be a canted antiferromagnet, as indicated by the behavior of the edge conductance in experiments with tilted magnetic fields [10]. However, as we argue below, these experiments are not sufficient to determine the proximity of graphene to

*Current address: Department of Physics, Massachusetts Institute of Technology, Cambridge, MA 02139, USA.
†macdpc@physics.utexas.edu
‡thierry.jolicoeur@u-psud.fr

the ideal SO(5) symmetric state. Even if graphene is in the antiferromagnetic side of the phase diagram, the presence of a weakly broken SO(5) symmetry would have important consequences, such as the existence of additional weakly gapped neutral collective modes as we will discuss in detail in Sec. IV and in Appendix D.

II. HAMILTONIAN SYMMETRIES

When projected to the $N = 0$ Landau level (LL) the graphene Hamiltonian is

$$\begin{aligned} H &= H_{\rm C} + H_{\rm v} + H_{\rm Z}, \\ H_{\rm C} &= \frac{1}{2}\sum_{i\neq j}\frac{e^2}{\epsilon|\vec{r}_i - \vec{r}_j|}, \\ H_{\rm v} &= \frac{1}{2}\sum_{i\neq j}\left[g_z\tau_z^i\tau_z^j + g_\perp\left(\tau_x^i\tau_x^j + \tau_y^i\tau_y^j\right)\right]\delta(\vec{r}_i - \vec{r}_j), \\ H_{\rm Z} &= -\epsilon_{\rm Z}\sum_i \sigma_z^i. \end{aligned} \tag{1}$$

In Eq. (1), $H_{\rm C}$ is the valley-independent Coulomb interaction, ϵ is an environment-dependent effective dielectric constant, $H_{\rm v}$ is the short-range valley-dependent interaction, $\tau_\alpha (\alpha = x,y,z)$ are Pauli matrices which act in valley space, $H_{\rm Z}$ is the Zeeman energy [1], $\epsilon_{\rm Z} = \mu_B B$ where μ_B is the Bohr magneton and B is the total magnetic field strength, and σ_α are Pauli matrices, which act in spin space. Note that B can have components both perpendicular and parallel to the graphene plane and that we have chosen the $\hat{z}$ direction in spin space to be aligned with B. The form used for $H_{\rm v}$ in Eq. (1) was proposed by Kharitonov [20,22].

The short-range interaction coupling constants $g_{z,\perp}/l_B^2$ are estimated to be $\sim a_0/l_B$ times the Coulomb energy scale $e^2/\epsilon l_B$, where $a_0 \sim 0.01 l_B$ is the lattice constant of graphene. They are therefore weak and physically relevant mainly when they lift low-energy Coulomb-only model degeneracies. For later notational convenience, we define the energy scales $u_{z,\perp} = g_{z,\perp}/(2\pi l_B^2)$. The Coulomb interaction $H_{\rm C}$ in Eq. (1) commutes with the fifteen SU(4) transformation generators which can be chosen as follows:

$$\begin{aligned} S_\alpha &= \frac{1}{2}\sum_i \sigma_\alpha^i, \qquad T_\alpha = \frac{1}{2}\sum_i \tau_\alpha^i, \\ N_\alpha &= \frac{1}{2}\sum_i \tau_z^i\sigma_\alpha^i, \quad \Pi_\alpha^\beta = \frac{1}{2}\sum_i \tau_\beta^i\sigma_\alpha^i, \end{aligned} \tag{2}$$

where the indices $\alpha = x,y,z$ and $\beta = x,y$. S_α and T_α are, respectively, the total spin and valley pseudospin. Due to the equivalence between valley and sublattice degrees of freedom in the $N = 0$ LL of graphene, N_α can be identified as a Néel vector. The physical meaning of the six Π_α^β operators is discussed below.

SU(4) symmetry is broken by the valley-dependent short-range interactions. At a generic point in the $(g_z, g_\perp)$ plane, $H_{\rm v}$ breaks the SU(4) symmetry down to $\mathrm{SU(2)_s \times U(1)_v}$ with the $\mathrm{U(1)_v}$ symmetry corresponding to conservation of the valley polarization T_z and the $\mathrm{SU(2)_s}$ symmetry corresponding to global spin-rotational invariance. Two high-symmetry lines

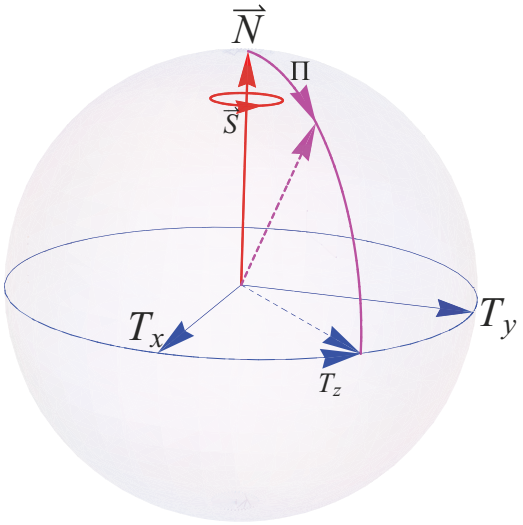

FIG. 1. (Color online) Schematic illustration of the five-component $(T_{x,y}, N_{x,y,z})$ order parameter space, and of rotations in this vector space produced by the SO(5) generators.

in the $(g_z, g_\perp)$ parameter space are evident: (1) for $g_\perp = 0$, the system is invariant under separate spin rotations in each valley yielding symmetry group $\mathrm{SU(2)_s^K \times SU(2)_s^{K'} \times U(1)_v}$ and (2) for $g_\perp = g_z$, there is a full rotational symmetry in valley space yielding symmetry group $\mathrm{SU(2)_s \times SU(2)_v}$. We have discovered that there is even higher symmetry along the $g_\perp = -g_z$ line where the generic $\mathrm{SU(2)_s \times U(1)_v}$ symmetry is enlarged to SO(5): see Appendix A for an explicit proof. Along this line, the Hamiltonian commutes with ten ($\vec{S}$, T_z, and the six Π operators) of the fifteen SU(4) generators identified in Eq. (2). The other five $(T_{x,y}, N_{x,y,z})$ SU(4) generators form a a natural order-parameter vector space on which the SO(5) group acts. As illustrated schematically in Fig. 1, spin operators $\vec{S}$ generate rotations in the Néel vector space $\vec{N}$, T_z generates rotations in the valley XY vector space $T_{x,y}$, and the Π operators generate rotations that connect these two spaces. When the Zeeman term is added to the Hamiltonian, the spin symmetry is limited to the invariance under rotations about the direction of the magnetic field. The symmetry groups of $H_{\rm C} + H_{\rm v}$ and H and the corresponding generators are listed in Table I.

As we will demonstrate, the SO(5) symmetry is spontaneously broken when it is exact. Provided that the Zeeman and short-range interaction terms, which explicitly break SO(5) symmetry, are not too strong, the $(T_{x,y}, N_{x,y,z})$ vectors can be used to construct a useful Ginzburg-Landau model or quantum effective-field theory. The Néel vector components of the order parameter characterize the AF part of the order, while the valley XY components capture the KD [18,20] part of the order. The SO(5) symmetry demonstrates that states which appear quite different at a first glance are close in energy and that they can be continuously transformed into one another by appropriate rotations in the SO(5) order parameter space. The 5D vector $(T_{x,y}, N_{x,y,z})$ identified here provides a concrete example for the 56 possible quintuplets proposed in graphene [23,24]. Although we focus here mainly

TABLE I. Expanded symmetries along high-symmetry lines in the $(g_z, g_\perp)$ plane. At a generic point in the $(g_z, g_\perp)$ plane, $H_C + H_v$ has $SU(2)_s \times U(1)_v$ symmetry and $H = H_C + H_v + H_Z$ has $U(1)_s \times U(1)_v$ symmetry.

	Symmetry of $H_C + H_v$	Generators	Symmetry of H	Generators
$g_\perp = 0$	$SU(2)_s^K \times SU(2)_s^{K'} \times U(1)_v$	S_α, N_α, T_z	$U(1)_s^K \times U(1)_s^{K'} \times U(1)_v$	S_z, N_z, T_z
$g_\perp = g_z$	$SU(2)_s \times SU(2)_v$	S_α, T_α	$U(1)_s \times SU(2)_v$	S_z, T_α
$g_\perp + g_z = 0$	SO(5)	$S_\alpha, T_z, \Pi_\alpha^x, \Pi_\alpha^y$	$U(1)_s \times SU(2)$	$S_z, T_z, \Pi_z^x, \Pi_z^y$

on monolayer graphene, a similar symmetry analysis applies to the $N = 0$ LL in bilayer graphene [25–27].

III. EXACT DIAGONALIZATION

We have performed exact diagonalization (ED) studies for the Hamiltonian specified in Eq. (1) acting in a $\nu = 0$ torus-geometry Hilbert space with up to $N_\phi = 8$ orbitals per flavor. When only Coulomb interactions are included, we verify that the ground state is a single Slater determinant with two occupied and two empty flavors [7]. The SU(4) multiplet structure of this broken-symmetry state is discussed in Appendix B. We specify the ratio of g_z to $g_\perp$ by the angle $\theta_g = \tan^{-1}(g_z/g_\perp)$ and fix the valley-dependent interaction strength $g/l_B^2 = \sqrt{g_\perp^2 + g_z^2}/l_B^2$ at $0.01e^2/(\epsilon l_B)$. Because gN_ϕ/l_B^2 is small compared to the Coulomb model charge-neutral energy gap that separates the ground state multiplet from the first excited multiplet at zero momentum, the role of the valley-dependent interactions is simply to lift the Coulomb model degeneracy and split the corresponding SU(4) ground state multiplet. Over the angle ranges $\theta_g \in [-\pi/4, \pi/2]$ and $\theta_g \in [5\pi/4, 7\pi/4]$, the exact ground states of $H_C + H_v$ are single-Slater determinants, with F and CDW orders, respectively. For other values of θ_g, valley-dependent interactions are nontrivial.

Figure 2 illustrates the θ_g dependence of the Hamiltonian spectrum for $N_e = 16$ electrons in $N = 0$ Landau levels with $N_\phi = 8$ over the $\theta_g \in [\pi/2, 5\pi/4]$ interval. Figure 2(a) plots ground state energies in various (S_z, T_z) sectors and demonstrates that the overall ground state has total valley polarization $T_z = 0$ and total spin $S = 0$ at all θ_g values in this range. Note that the dependence of energy on T_z is suppressed as the CDW state is approached ($\theta_g \to 5\pi/4$) and that the dependence of energy on S is suppressed as the F state is approached ($\theta_g \to \pi/2$). Figure 2(b) illustrates how the $T_z = 0$ sector of the SU(4) Coulomb ground-state multiplet is split by H_v. Since H_v preserves $SU(2)_s$ spin symmetry, all energies in Figs. 2(a) and 2(b) occur in $SU(2)_s$ multiplets. At $\theta_g = 3\pi/4$, eigenvalues with different values of S merge to form SO(5) multiplets, each forming an irreducible representation of the SO(5) group. (A geometric representation of the SO(5) multiplet structure is provided in Appendix B). All eigenstates have a definite value of the SO(5) Casimir operator [28] $\Gamma^2 = S^2 + T_z^2 + \Pi^2 = l(l+3)$, with integer $l = 0, 1, \ldots, N_\phi$. The low-energy spectrum at $\theta_g = 3\pi/4$ is accurately fit by the following equation:

$$H_v^{\text{eff}}\left(\theta_g = \frac{3\pi}{4}\right) = u_z\left[\frac{2\Gamma^2}{N_\phi + 1} - \frac{N_\phi(N_\phi + 5)}{N_\phi + 1}\right], \qquad (3)$$

implying that the ground state, $|G(3\pi/4)\rangle$, is a SO(5) singlet with $\Gamma^2 = 0$. It follows that the 5D order parameter vector

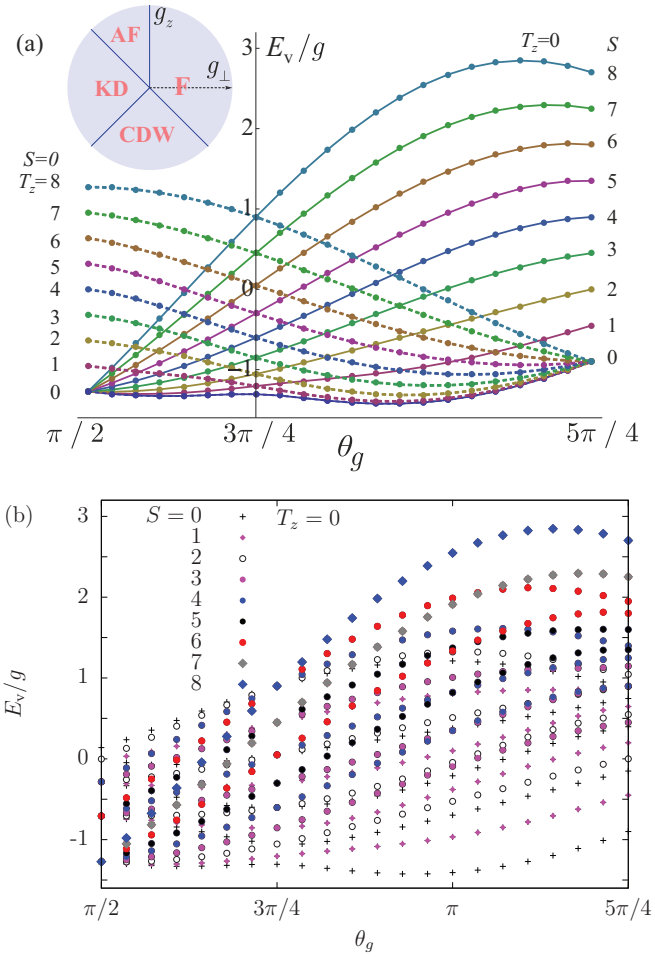

FIG. 2. (Color online) Low-energy spectrum on the torus geometry for zero total momentum, filling factor $\nu = 0$, and orbital Landau level degeneracy $N_\phi = 8$ as a function of θ_g in the range $[\pi/2, 5\pi/4]$. E_v is defined as the difference between the eigenvalues of $H_C + H_v$ and the Coulomb-only ground state energy. All plotted eigenvalues are degenerate in the absence of H_v. (a) Ground-state energies in a series of (T_z, S) sectors. The solid lines show the *lowest* $T_z = 0$ energies for different total spin S values. Similarly, the dashed lines show the *lowest* spin singlet ($S = 0$) energies in different T_z sectors. The ground state has $S = 0$ and $T_z = 0$ throughout the plotted θ_g range. The inset shows the mean-field phase diagram over the full θ_g range from Ref. [20]. (b) Low-energy states in the $T_z = 0$ sector for a series of total spin S quantum numbers. Note that at $\theta_g = 3\pi/4$, states with different S values are degenerate because of the hidden SO(5) symmetry.

$(T_{x,y}, N_{x,y,z})$ is maximally polarized:

$$\left\langle T_x^2 + T_y^2 + N^2 \right\rangle_{3\pi/4} = \langle C_4 - \Gamma^2 \rangle_{3\pi/4} = \langle C_4 \rangle_{3\pi/4} \approx C_4^*, \tag{4}$$

where $\langle \cdots \rangle_{3\pi/4}$ denotes expectation values in the ground state $|G(3\pi/4)\rangle$ and $C_4^* = N_\phi(N_\phi + 4)$ is the value of the SU(4) Casimir operator C_4 in the Coulomb model SU(4) multiplet. The approximation leading to C_4^* in Eq. (4) is validated by numerical calculation, and also follows from the argument that $|G(3\pi/4)\rangle$ is adiabatically connected to a state in the SU(4) multiplet. Because $|G(3\pi/4)\rangle$ does not break SO(5) symmetry, $\langle N_\alpha^2 \rangle_{3\pi/4} = \langle T_\beta^2 \rangle_{3\pi/4} \approx C_4^*/5$ with $\alpha = x,y,z$ and $\beta = x,y$.

Equation (3) predicts that in the thermodynamic limit $N_\phi \to \infty$, small l multiplets will approach degeneracy. By making an analogy with the quantum rotor model, we can see that this property signals spontaneous SO(5) symmetry breaking. The energy in Eq. (3) can be interpreted as the kinetic energy of a generalized rotor model in the 5D $(T_{x,y}, N_{x,y,z})$ space with the SO(5) generators playing the role of angular momenta. In the thermodynamic limit $N_\phi \to \infty$, the moments of inertia of the rotors diverge and it can be stuck in a spontaneously chosen direction, resulting in symmetry breaking. The absence of ground state level crossings along the $\theta_g = 3\pi/4$ line in Fig. 2 indicates that the crossover between AF and KD states is smooth in finite-size systems. However, the level crossings between the low-lying excited states in Fig. 2 signals a first-order phase transition in the thermodynamic limit.

IV. LOW-ENERGY EFFECTIVE THEORY AND COLLECTIVE MODES

Following Refs. [20,29,30], we can derive a low-energy effective-field theory for $\nu = 0$ quantum Hall states by constructing the Lagrangian,

$$L = \langle \psi | i\partial_t - H | \psi \rangle = \int \frac{\mathrm{d}^2\mathbf{r}}{2\pi l_B^2} [\mathcal{B} - \mathcal{H}], \tag{5}$$

where $|\psi\rangle$ is a Slater-determinant state in which two orthogonal occupied spinors $\chi_{1,2}$ are allowed to vary slowly in space and time. The Lagrangian density $\mathcal{L} = \mathcal{B} - \mathcal{H}$ has kinetic Berry phase $[\mathcal{B} = i(\chi_1^\dagger \partial_t \chi_1 + \chi_2^\dagger \partial_t \chi_2)]$ and energy-density $\mathcal{H}$ contributions. As detailed in Appendix C we find that

$$\begin{aligned}\mathcal{H} = {} & -u_\perp - 2\epsilon_Z s_z + (u_z + u_\perp)\left(t_z^2 - \sum_{\alpha=x,y,z} s_\alpha^2\right) \\ & + 2u_\perp \sum_{\beta=x,y} t_\beta^2 + (u_\perp - u_z) \sum_{\alpha=x,y,z} n_\alpha^2 \\ & + l_B^2 \Bigg[\rho_z (\nabla t_z)^2 + \rho_\perp \sum_{\beta=x,y} (\nabla t_\beta)^2 + \sum_{\alpha=x,y,z} \rho_s (\nabla s_\alpha)^2 \\ & + \rho_n (\nabla n_\alpha)^2 + \rho_\pi \left(\left(\nabla \pi_\alpha^x\right)^2 + \left(\nabla \pi_\alpha^y\right)^2 \right) \Bigg].\end{aligned} \tag{6}$$

The stiffness coefficients $\rho_z = \rho_0 - (3u_z + 2u_\perp)/4$, $\rho_\perp = \rho_0 - (u_z + u_\perp)/4$, $\rho_s = \rho_0 + (u_z + 2u_\perp)4$, $\rho_n = \rho_0 + (u_z - 2u_\perp)/4$ and $\rho_\pi = \rho_0 - u_z/4$, are dominated by the common Coulomb contribution $\rho_0 = \sqrt{2\pi} e^2/(16\epsilon l_B)$. It is easy to check that the energy density function $\mathcal{H}$ has the same symmetries as the Hamiltonian H. The mean-field theory ground state is determined by assuming that all fields are static and spatially uniform. The energy competitions behind the mean-field phase diagram previously derived by Kharitonov [20] are transparent when Eq. (6) is combined with the normalization constraint $\sum_\alpha (t_\alpha^2 + n_\alpha^2 + s_\alpha^2 + (\pi_\alpha^x)^2 + (\pi_\alpha^y)^2) = 1$ (see Appendix C). In the absence of a Zeeman field the four mean-field phases are the F state ($\sum s_\alpha^2 = 1$), the AF state ($\sum n_\alpha^2 = 1$), the KD state ($t_x^2 + t_y^2 = 1$), and the CDW state ($t_z^2 = 1$). The phase boundaries between these states, shown in the inset of Fig. 2(a), lie along the high symmetry lines identified in Table I.

We now concentrate on physics near $u_z + u_\perp = 0$ where a first order phase transition occurs between KD and AF states and the system exhibits SO(5) symmetry. The $u_z + u_\perp = 0$ line in graphene is analogous to the $J_{xy} = J_z$ line in a XXZ spin model, along which a phase transition occurs between Ising and XY ground states and the system exhibits expanded O(3) symmetry. One physical manifestation of SO(5) symmetry along the transition line is the response to an external Zeeman field, which induces a finite z direction spin polarization s_z. It follows from orthogonality constraints on the fields discussed in Appendix C that when among the ten SO(5) generators only s_z has a finite expectation value, $t_{x,y}$ and n_z must vanish. A finite Zeeman energy therefore favors the AF state over the KD state because the AF state can distort to a canted AF with a finite s_z and a Néel vector lying in the xy plane. A sufficiently strong Zeeman field eventually favors the F state. Because experiments detect what appears to be a continuous phase transition as a function of Zeeman coupling strength [10], they suggest that the ground state in the absence of Zeeman coupling lies in the AF region of the phase diagram.

Close to the $u_z + u_\perp = 0$ line, the system retains crucial SO(5) properties in the presence of a small Zeeman term. Approximate SO(5) symmetry is revealed in the collective mode spectra of both KD and AF states. The KD phase spontaneously breaks the valley $\mathrm{U(1)_v}$ symmetry. Choosing the ground state to have valley polarization t_x with a spontaneous nonzero value, we see that infinitesimal SU(4) rotations [31] give rise to infinitesimal values of eight fields, $\{t_{y,z}, n_{x,y,z}, \pi^y_{x,y,z}\}$, and leave the remaining six fields, $\{s_{x,y,z}, \pi^x_{x,y,z}\}$ at zero. The eight dynamical fields parametrize the tangent manifold of the mean-field ground state. By evaluating the Berry phase, we find that for small fluctuations the valley pseudospin fields t_y and t_z are canonically conjugate, and that the Néel vector field n_α is conjugate to π_α^y. The valley pseudospin and Néel vector collective modes therefore decouple. The valley collective mode is gapless because of the Kekulé state's broken U(1) symmetry and has dispersion

$$\omega_1(\mathrm{KD}) = 2k\sqrt{\rho_\perp(u_z - u_\perp + \rho_z k^2)}, \tag{7}$$

where k is wave vector and lengths are in units of l_B. The three additional collective modes are kinetically coupled Néel-π modes and have energy

$$\omega_{2,3,4}(\mathrm{KD}) = 2\sqrt{(|u_z + u_\perp| + \rho_n k^2)(2|u_\perp| + \rho_\pi k^2)}. \tag{8}$$

Note that these modes become gapless as the SO(5) symmetry line is approached and the energy cost of Néel fluctuations away from the KD state vanishes, and that the Zeeman

field does not influence collective mode energies in the KD phase because s_z is not a dynamical field. Similarly, the AF state spontaneously breaks the spin SU(2)$_s$ symmetry. When the Néel vector is chosen to lie along the x axis, the dynamical fields generated by infinitesimal SU(4) rotations are $\{s_{y,z}, n_{y,z}, t_{x,y}, \pi_x^{x,y}\}$. Evaluating the Berry phase, we find that s_y is conjugate to n_z and s_z to n_y, as in a standard antiferromagnet. The spin-collective modes are

$$\omega_{1,2}(\mathrm{AF}) = 2k\sqrt{\rho_n(2|u_\perp| + \rho_s k^2)}. \quad (9)$$

In the AF state, (t_x, π_x^y) and (t_y, π_x^x) fluctuations form kinetically coupled conjugate pairs and give rise to the sublattice/π collective mode energies:

$$\omega_{3,4}(\mathrm{AF}) = 2\sqrt{(u_z + u_\perp + \rho_\perp k^2)(u_z - u_\perp + \rho_\pi k^2)}. \quad (10)$$

Note that all four collective modes are gapless and degenerate along the $u_z + u_\perp = 0$ line. The degeneracy arises from the SO(5) symmetry. Appendix D describes how the collective modes in Eqs. (9) and (10) are modified by the Zeeman field.

V. DISCUSSION AND SUMMARY

In ordered systems a Landau-Ginzburg or quantum effective model which includes a single-order parameter, for example, a complex pair-amplitude order parameter for a superconductor or a magnetization direction order parameter for a magnetic system, is often able to describe thermodynamic, fluctuation, and response properties over wide ranges of temperature and experimentally tunable system parameters. These theories can be powerfully predictive even when their parameters cannot be reliably calculated from the underlying microscopic physics. The naive effective-field-theory approach sometimes fails however. A notable example is the case of high-temperature superconductors in which experiments indicate that charge-density, spin-density, and pair-amplitude order parameters have correlated quantum and thermal fluctuations that must be treated simultaneously. Unlike the case discussed in the present paper in which an $N = 5$ component effective theory can be motivated and its parameters estimated on the basis of microscopic physics, large-N field theories [21,32,33] are typically constructed on the basis of hints from experimental data, for example, from observed correlations in the temperature and parameter dependence of the fluctuation amplitudes of different observables. In these theories, it is often difficult to be certain that all relevant fields have been identified, and to identify constraints imposed on the fluctuations of these fields by the underlying microscopic physics. As discussed below, the remarkably simple example of ordered states in graphene quantum Hall systems, particularly ordered states at $\nu = 0$, suggests criteria which can be tested experimentally to validate large-N unified theories of systems with competing orders.

As summarized in Table II, there is a close analogy between SO(5) symmetry in the quantum Hall effect of graphene and SO(5) symmetry in some theories of high-T_c superconductivity (HTS) [21]. The SO(5) theory of HTS theory unifies antiferromagnetism and d-wave superconductivity (dSC). The analog of d-wave superconductivity in the graphene quantum Hall case is Kekulé distortion order. The order parameters of both theories involve a sublattice degree of freedom, the honeycomb sublattice degree-of-freedom in the case of graphene and the sublattice degree of freedom of the magnetically ordered state in HTS SO(5) theory case. The graphene analog of the chemical potential μ term, which tunes transitions between antiferromagnetic and d-wave superconducting states in the HTS case, is a sublattice-staggered potential ϵ_v. Interestingly this field is easily tunable experimentally [34–37] in the bilayer graphene case. SO(5) symmetry in HTS is conjectured to emerge in low-energy effective theory [21], and can be exactly realized in extended Hubbard model with artificial long-range interactions [38,39]; however, it never becomes exact for commonly used models like t-J or Hubbard model. In contrast, SO(5) symmetry and its explicit symmetry breaking naturally appear in the microscopic Hamiltonian [Eq. (1)] for the quantum Hall effect in graphene at any filling factors within $N = 0$ LL. We note that generic SO(5) symmetry without any fine-tuning parameters can appear in a spin-3/2 ultracold femionic system [40,41].

TABLE II. Comparison between the Kekulé-distortion state in graphene and the d-wave state in high-temperature superconductors.

Parameter	Kekulé-distortion state	d-wave state
Order Parameter	(T_x, T_y)	(Δ_x, Δ_y)
U(1) generator	T_z	Charge Q
External Potential	Staggered potential ϵ_v	Chemical potential μ

The SO(5) symmetry in graphene is manifested by a multiplet structure in the exact diagonalization spectra, and by the appearance of soft collective modes beyond those associated with Kekulé or antiferromagnetic order. In particular, the antiferromagnetic state of graphene has π-operator fluctuation collective modes. The observation of the analogous collective modes in the antiferromagnetic state of high-temperature superconductors would provide powerful evidence for the applicability of an effective theory, which unifies antiferromagnetism and superconductivity only. On the other hand, their absence would likely indicate that an effective theory of this type is not adequate over a useful range of the tunable doping-level parameter of HTSs. Similarly, a recently proposed alternate $N = 6$ parameter theory [32], which unifies charge-density-wave and d-wave superconducting order, also has implications for the collective mode structure, which, if verified, would provide a powerful validation.

Finally, we would like to comment on the relevance of our study to the understanding of the highly insulating quantum Hall state found in graphene at neutrality. Experiments with tilted magnetic fields [10] are consistent with the view that the state at neutrality is a canted antiferromagnet. Since the transition between a canted antiferromagnet and the spin polarized state is controlled solely by the ratio of the Zeeman term to the $u_\perp$ interaction strength [20], these very experiments serve to estimate the value of $u_\perp$, which is found to be about $u_\perp \sim -10\epsilon_Z$ [11,12]. This experiment, however, does not serve to estimate the value of u_z, but simply to constrain it to satisfy $u_z \gtrsim |u_\perp|$, from the requirement that the system is in the canted antiferromagnet phase. The determination of the value of u_z, relevant for monolayer graphene and, hence, of its proximity to the ideal SO(5) symmetric state,

is therefore an open experimental problem. The presence of a weakly broken SO(5) symmetry would have important physical consequences, such as the existence of additional weakly gapped neutral collective modes as we illustrated in Sec. IV and in Appendix D.

ACKNOWLEDGMENTS

This work was supported by the DOE Division of Materials Sciences and Engineering under Grant DE-FG03-02ER45958, and by the Welch foundation under Grant TBF1473. We gratefully thank Texas Advanced Computing Center (TACC) and IDRIS-CNRS Project 100383 for providing technical assistance and computer time allocations.

APPENDIX A: PROOF OF SO(5) SYMMETRY FOR $g_z + g_\perp = 0$

Let us first briefly review how SO(5) arises naturally as a subgroup of SU(4). The fifteen generators of SU(4) can be chosen to be the Pauli matrices in spin and valley space and their direct products: $\{\sigma_\alpha, \tau_\beta, \sigma_\alpha\tau_\beta\}$. The Clifford algebra, $\{\gamma_\mu, \gamma_\nu\} = 2\delta_{\mu\nu}$, is realized by a subset of these generators, namely the 4×4 γ matrices, which can be chosen as

$$\gamma_1 = \tau_x, \quad \gamma_2 = \tau_z\sigma_x, \quad \gamma_3 = \tau_z\sigma_y, \quad \gamma_4 = \tau_z\sigma_z, \quad \gamma_5 = \tau_y. \tag{A1}$$

SO(5) can be shown to be generated by the commutators of these γ matrices: $[\gamma_\mu, \gamma_\nu]$. More specifically, we have the following ten generators of SO(5):

$$\gamma_{ab} = -\frac{i}{2}[\gamma_a, \gamma_b], \tag{A2}$$

which can be thought of as a 5×5 antisymmetric tensor

$$\gamma_{ab} = \begin{pmatrix} 0 & & & & \\ \tau_y\sigma_x & 0 & & & \\ \tau_y\sigma_y & -\sigma_z & 0 & & \\ \tau_y\sigma_z & \sigma_y & -\sigma_x & 0 & \\ -\tau_z & \tau_x\sigma_x & \tau_x\sigma_y & \tau_x\sigma_z & 0 \end{pmatrix}. \tag{A3}$$

These matrices satisfy the following commutation relations:

$$[\gamma_{ab}, \gamma_{cd}] = 2i(\delta_{ac}\gamma_{bd} + \delta_{bd}\gamma_{ac} - \delta_{ad}\gamma_{bc} - \delta_{bc}\gamma_{ad}), \tag{A4}$$

$$[\gamma_{ab}, \gamma_c] = 2i(\delta_{ac}\gamma_b - \delta_{bc}\gamma_a). \tag{A5}$$

Equation (A4) shows that the ten independent γ_{ab} matrices obey a set of closed commutation relations, which is the SO(5) Lie algebra. Additionally, according to Eqs. (A4) and (A5), when the group is viewed as acting on γ_{ab} and γ_a by matrix conjugation, we have, respectively, a tensor and a vector representation of SO(5) [42].

We will now demonstrate explicitly that SO(5) is an exact symmetry of the Hamiltonian in the absence of Zeeman coupling for $g_z + g_\perp = 0$. From among the fifteen generators of SU(4) identified in the main text, the spin operator S_α, the valley polarization operator T_z and the Π^β_α operators are the ten generators of the SO(5) group. S_α and T_z automatically commute with H_v for any values of g_z and $g_\perp$. Thus SO(5) will be a symmetry group if the six Π^β_α operators also commute with H_v. To simplify the calculation of these commutators, we define the Π ladder operators:

$$\Pi^\lambda_{\lambda'} = \sum_i \tau^i_\lambda \sigma^i_{\lambda'}, \quad \Pi^\lambda_z = \sum_i \tau^i_\lambda \sigma^i_z, \tag{A6}$$

where λ and λ' can be $+$ or $-$. $\tau_\pm = (\tau_x \pm i\tau_y)/2$ are ladder operators in valley space, and the spin ladder operators $\sigma_\pm$ are similarly defined. We work out the commutator $[\Pi^+_+, H_v]$ in detail below:

$$\begin{aligned}
[\Pi^+_+, H_v] &= 2\sum_{i\neq j}\left(-g_z\tau^j_z\tau^i_+\sigma^i_+ + g_\perp\tau^j_+\tau^i_z\sigma^i_+\right)\delta(\vec{r}_i - \vec{r}_j) \\
&= 2\sum_{v,s}\sum_{p_1p_2p_3p_4}\tau^{vv}_z D_{p_1p_2p_3p_4}\left(-g_z c^\dagger_{p_1K\uparrow}c^\dagger_{p_2vs}c_{p_3vs}\right. \\
&\quad \left.\times c_{p_4K'\downarrow} + g_\perp c^\dagger_{p_1v\uparrow}c^\dagger_{p_2Ks}c_{p_3K's}c_{p_4v\downarrow}\right) \\
&= 2(g_z + g_\perp)\sum_{p_1p_2p_3p_4} D_{p_1p_2p_3p_4}\left(c^\dagger_{p_1K\uparrow}c^\dagger_{p_2K'\uparrow}c_{p_3K'\uparrow}\right. \\
&\quad \left.\times c_{p_4K'\downarrow} + c^\dagger_{p_1K\uparrow}c^\dagger_{p_2K\downarrow}c_{p_3K'\downarrow}c_{p_4K\downarrow}\right).
\end{aligned} \tag{A7}$$

The second line of Eq. (A7) is the Landau gauge second quantized form of the first line. $c^\dagger_{pvs}$ (c_{pvs}) is an electron creation (annihilation) operator, p denotes the orbital index within the $N = 0$ Landau level, $v = K, K'$ labels valley, and $s = \uparrow, \downarrow$ labels spin. $D_{p_1p_2p_3p_4}$ is the orbital two-particle matrix element for the δ function interaction:

$$\begin{aligned}
D_{p_1p_2p_3p_4} &= \int\int d\vec{r}_1 d\vec{r}_2\, \phi^*_{p_1}(\vec{r}_1)\phi^*_{p_2}(\vec{r}_2)\delta(\vec{r}_1 - \vec{r}_2)\phi_{p_3}(\vec{r}_2) \\
&\quad \times\phi_{p_4}(\vec{r}_1) \\
&= \int d\vec{r}\; \phi^*_{p_1}(\vec{r})\phi^*_{p_2}(\vec{r})\phi_{p_3}(\vec{r})\phi_{p_4}(\vec{r}),
\end{aligned} \tag{A8}$$

where $\phi_p(\vec{r})$ is the wave function for orbital p. In the simplification leading to the last line of Eq. (A7), we used (i) fermion anticommutation relations, and (ii) the identity $D_{p_1p_2p_3p_4} = D_{p_1p_2p_4p_3}$, which is a special property of δ function interaction. Equation (A7) shows that $[\Pi^+_+, H_v] = 0$ at $g_z + g_\perp = 0$. In a similar fashion, it can be shown that the other Π operators also commute with H_v at $g_z + g_\perp = 0$. Thus H_v has the exact SO(5) symmetry for $g_z + g_\perp = 0$ independent of filling factors. The symmetry follows from the short-range nature of the valley-symmetry breaking interaction combined with the Pauli exclusion principle for electrons. Note that in Eq. (A7), we did not make use of the explicit form of the wave function $\phi_p(\vec{r})$. The same Hamiltonian in Eq. (1) has also been used to describe the physics in $N = 0$ LL of bilayer graphene(BLG) [25–27]. There is a similar equivalence among valley, sublattice, and layer degrees of freedom within $N = 0$ LL in BLG. The main difference is that $N = 0$ LL in BLG contains both $n = 0$ and $n = 1$ magnetic oscillator states. Since the SO(5) symmetry identified for the Hamiltonian in Eq. (1) is independent of the single-particle wave function basis, it can also be applied to the case of BLG.

APPENDIX B: EXACT DIAGONALIZATION RESULTS

Our ED results for finite-size systems with up to 16 electrons verify that the ground state at $\nu = 0$ for Coulomb

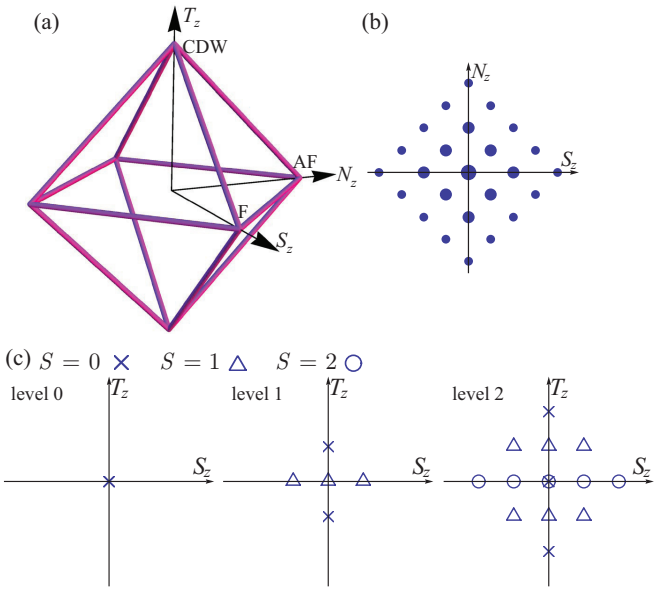

FIG. 3. (Color online) Geometric representation of SU(4) multiplet structures. (a) The octahedron in (S_z, N_z, T_z) space represents the SU(4) multiplet structure of Coulomb ground states at $\nu = 0$. (b) A T_z-constant plane in the octahedron displayed for $T_z = N_\phi - 4$ reached by applying lowering operators to the CDW state with $T_z = N_\phi$. The size of the symbols indicates the degeneracy at each point in the (S_z, N_z) plane. (c) Multiplet structures of the first three levels of SO(5).

interactions only ($H = H_C$) is given exactly by mean-field theory. The ground-state wave functions at $\nu = 0$ are single Slater determinants with filled Landau levels for two of four flavors. This property is a generalization of simple, quantum Hall ferromagnetism, the occurrence of spontaneously spin-polarized states at odd filling factors when the spin degree-of-freedom is added to the physics of a parabolic band system Landau levels. We have used periodic boundary conditions and classified many-body states by their magnetic translation symmetries [43]. In graphene, the $\nu = 0$ ground states occur at zero momentum and form an irreducible representation of SU(4).

The $\nu = 0$ F, AF, and CDW states are included in the ground-state multiplet and can be expressed in the form

$$|\chi_{1,2}\rangle = \prod_{p=1}^{N_\phi} c^\dagger_{p\chi_1} c^\dagger_{p\chi_2} |0\rangle, \tag{B1}$$

where $\chi_{1,2}$ are the two spinors defining the state and p is the index of the LL orbital. When considered as a tensor representation of SU(4), this formula implies that the states in this multiplet are tensors with $2N_\phi$ indices in two symmetric sets each with N_ϕ indices, i.e., they are described by the Young tableau:

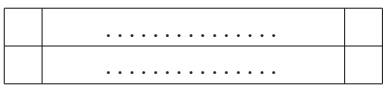

with N_ϕ columns and two rows. Figure 3(a) represents the SU(4) multiplet structure geometrically in terms of an octahedron in (S_z, N_z, T_z) space [44]. The octahedral shape is understood to bound a tetrahedral lattice of points in which each point designates the states within the multiplet with common S_z, N_z, T_z quantum numbers. Figure 3(b) shows a slice of this lattice with $T_z = N_\phi - 4$. F, AF and CDW states are located at vertices of the octahedron, and other orthogonal degenerate states are derived from them by applying suitable SU(4) transformations.

States in the SU(4) ground-state multiplet share the same value of the SU(4) guadratic Casimir operator:

$$C_4 = S^2 + N^2 + T^2 + \Pi^2, \tag{B2}$$

where $S^2 = \sum_{\alpha=x,y,z} S_\alpha^2$, N^2 and T^2 are similarly defined, and $\Pi^2 = \sum_{\alpha=x,y,z} (\Pi_\alpha^x)^2 + (\Pi_\alpha^y)^2$. C_4 takes value $N_\phi(N_\phi + 4)$ for the Coulomb ground-state multiplet at $\nu = 0$. Figure 3(b) demonstrates that there can be more than one state in the multiplet at a given (S_z, N_z, T_z) point. Hence, an additional quantum number, such as $S^2 + N^2$, is needed to uniquely label a state within the SU(4) multiplet of interest [44]. $S^2 + N^2$ is one of the quadratic Casimir operator of the $SU(2)_s^K \times SU(2)_s^{K'}$ subgroup of SU(4). We note that $SU(2)_s^K \times SU(2)_s^{K'}$ group has another quadratic Casimir operator $\sum_{\alpha=x,y,z} S_\alpha N_\alpha$, which is identical to 0 for Coulomb ground states at $\nu = 0$.

SU(4) symmetry is lifted by the valley-symmetry breaking interaction H_v, and the octahedral multiplet is split. At $\theta_g = 3\pi/4$, SU(4) symmetry is reduced to SO(5) symmetry. Figure 3(c) shows the SO(5) multiplet structure of the three lowest energy states, which coincide with the lowest degeneracies. Within a level, states are distinguished by T_z, S_z and total spin S quantum numbers, and share the same value of the SO(5) Casimir operator $\Gamma^2 = S^2 + T_z^2 + \Pi^2 = l(l+3)$, l being a nonnegative integer. We note that the same SO(5) multiplet structure has arisen previously in numerical studies of the t-J model [45]. Interestingly, along the SO(5) line, i.e., for $\theta_g = 3\pi/4$, we find numerically that the eigenenergies are linear in Γ^2, as illustrated in Fig. 4(a). The low-energy part of the spectrum along the SO(5) line is accurately fit by the following equation:

$$H_v^{\text{eff}}\left(\theta_g = \frac{3\pi}{4}\right) = u_z\left[\frac{2\Gamma^2}{N_\phi + 1} - \frac{N_\phi(N_\phi + 5)}{N_\phi + 1}\right]. \tag{B3}$$

The ground state at $\theta_g = 3\pi/4$ is an SO(5) singlet with $\Gamma^2 = 0$.

Away from $\theta_g = 3\pi/4$, SO(5) symmetry is explicitly broken, leading to anisotropy in the 5D space. Interestingly, the spectrum can also be fit by a linear form in the appropriate quadratic Casimir operators along other high symmetry lines. For example, at $\theta_g = \pi/2$, the Casimir operators of the corresponding symmetry group $SU(2)_s^K \times SU(2)_s^{K'} \times U(1)_v$ are $S^2 + N^2$ and T_z^2. For a T_z−constant plane shown in Fig. 3(b), $S^2 + N^2$ takes values $f(f+2)$, with non-negative $f = N_\phi - |T_z|, N_\phi - |T_z| - 2, \cdots$. In analogy with the $\theta_g = 3\pi/4$ case, the low-energy spectrum at $\theta_g = \pi/2$ is accurately fit by

$$H_v^{\text{eff}}\left(\theta_g = \frac{\pi}{2}\right) = u_z \frac{T_z^2 - (S^2 + N^2) + N_\phi}{N_\phi + 1}. \tag{B4}$$

By interpolating between Eqs. (B3) and (B4), we arrive at an expression which describes the low-energy spectrum of the SU(4) ground state manifold over the full $\theta_g \in (\pi/2, 5\pi/4)$

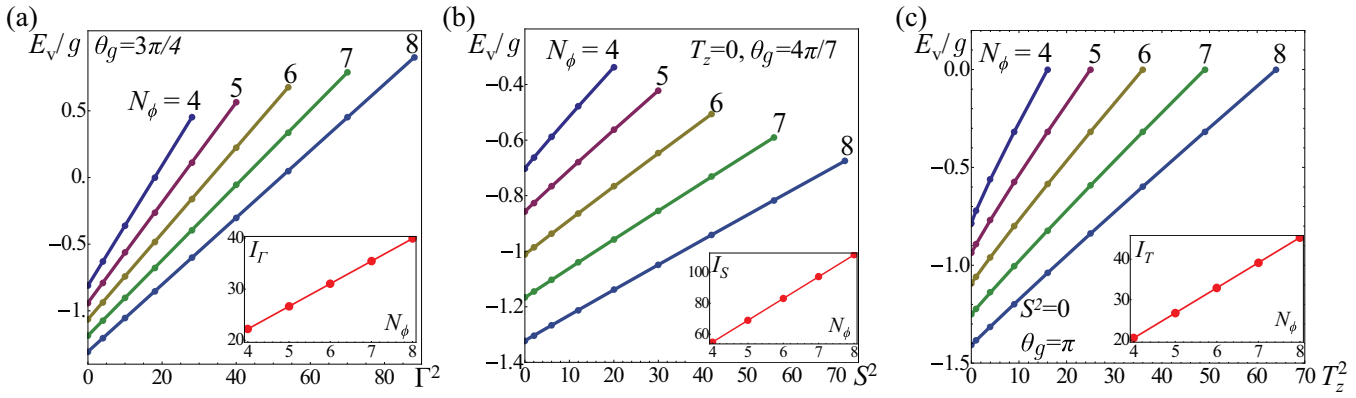

FIG. 4. (Color online) Finite size scaling analysis. (a) E_v/g at $\theta_g = 3\pi/4$ as a function of Γ^2 for N_ϕ ranging from 4 to 8. (b) In a given $(T_z = 0, S)$ sector, the *lowest* energy at $\theta_g = 4\pi/7 \in [\pi/2, 3\pi/4]$ as a function of S^2. (c) In a given $(S = 0, T_z)$ sector, the *lowest* energy at $\theta_g = \pi$ as a function of T_z^2. The inset in each figure shows the inverse of slope vs N_ϕ. See text for a more detailed description.

interval:

$$H_v^{\text{eff}} = \frac{1}{N_\phi + 1}\big[-2u_\perp\Gamma^2 + (u_z + u_\perp)\big(T_z^2 - S^2 - N^2\big) + u_z N_\phi + u_\perp N_\phi(N_\phi + 6)\big]. \tag{B5}$$

Equation (B5) is limited in two ways: (1) it describes only the low-energy part of the spectrum which evolves adiabatically from the SU(4) ground state multiplet, and (2) it is obtained by fitting numerical data at the high-symmetry points $\theta_g = \pi/2$ and $3\pi/4$. The SO(5) symmetry-breaking states at $\theta_g = 3\pi/4$ were discussed in the main text.

Equation (B5) makes the nature of the transition betwen AF and Kekulé phases at $\theta_g = 3\pi/4$ clear. As illustrated in Fig. 2(a) and discussed in the main text, the ground state throughout the entire $\theta_g \in (\pi/2, 5\pi/4)$ range is singly degenerate and has $S^2 = 0$ and $T_z = 0$. Therefore, on the $\theta_g < 3\pi/4$ side of the SO(5) line, the quantity $-(u_z + u_\perp)N^2$ in Eq. (B5) is an easy-plane anisotropy in the 5D space with the Néel vector space being the easy-plane; Néel order is favored over Kekulé order for $\theta_g < 3\pi/4$. On the $\theta_g > 3\pi/4$ side of SO(5) point, the Kekulé state is favored and the $T_{x,y}$ vectors lie in the easy plane. We conclude that there is a spin-flop phase transition in the 5D space across the SO(5) point. The phase transition is of first order. Our analysis is in agreement with the mean-field prediction of a zero temperature first-order phase transition and places it on rigorous grounds.

We will now describe how the finite size scaling demonstrates the existence of spontaneous symmetry-breaking away from the SO(5) point. In Fig. 4(b), we plot the lowest energy at a representative angle $\theta_g = 4\pi/7$ in different $(T_z = 0, S)$ sectors as a function of S^2 for N_ϕ from 4 up to 8. There is good linear relationship between the plotted energy and S^2. The quantity I_S, defined as the inverse of the slope, increases linearly as N_ϕ increases. This quantity is a generalized moment of inertia and its divergence indicates spontaneous $SU(2)_s$ symmetry breaking in the thermodynamic limit at $\theta_g = 4\pi/7$. The reasoning is analogous as that for the SO(5) symmetry breaking at $\theta_g = 3\pi/4$. In Fig. 4(c), a similar scaling analysis is applied to the spin singlet sector with varying T_z numbers at $\theta_g = \pi$. In this case, the analysis signals a spontaneous $U(1)_v$ symmetry breaking in the thermodynamic limit. We remark that the finite-size scaling behavior in our system is very similar to that in the two-dimensional antiferromagnetic Heisenberg model. The ground state of the latter model is a spin singlet [46] in any finite size system. However, low-lying energy levels collapse to the ground state in the thermodynamical limit, resulting in spontaneous symmetry breaking [47,48]. This set of low-lying states is often referred to as a *tower of states*.

So far, the Zeeman field has been neglected. Since S_z has been chosen as a good quantum number in our exact diagonalization calculations, the Zeeman field simply shifts the energy of a state by an amount proportional to its S_z value. We found that the mean-field phase boundary between canted antiferromagnetic state and KD in the presence of a Zeeman field is in quantitative agreement with exact diagonalization results for $N_\phi = 8$.

APPENDIX C: LOW-ENERGY EFFECTIVE THEORY

The continuum model Lagrangian

$$L = \langle\psi|i\partial_t - H|\psi\rangle = \int \frac{d^2\mathbf{r}}{2\pi l_B^2}\,[\mathcal{B} - \mathcal{H}], \tag{C1}$$

where $|\psi\rangle$ is a Slater-determinant state in which two orthogonal occupied spinors $\chi_{1,2}$ are allowed to vary slowly in space and time. The Lagrangian density $\mathcal{L} = \mathcal{B} - \mathcal{H}$ has a Berry phase part

$$\mathcal{B} = i(\chi_1^\dagger\partial_t\chi_1 + \chi_2^\dagger\partial_t\chi_2) \tag{C2}$$

and an energy density contribution

$$\mathcal{H} = l_B^2\mathcal{E}_0(\nabla P) + \mathcal{E}_v(P) - \frac{l_B^2}{2}\mathcal{E}_v(\nabla P) + \mathcal{E}_Z(P), \tag{C3}$$

where P is the local density matrix, $P = \chi_1\chi_1^\dagger + \chi_2\chi_2^\dagger$ and $\mathcal{E}_0(\nabla P)$ is the contribution from the SU(4) symmetric Coulomb interaction, which is nonzero only when P is space dependent:

$$\mathcal{E}_0(P) = \rho_0 \text{Tr}[\nabla P \nabla P], \tag{C4}$$

with stiffness $\rho_0 = \sqrt{2\pi}e^2/(16\epsilon l_B)$. The next two terms are contributed by the valley-dependent interactions:

$$\mathcal{E}_{\rm v}(P) = \frac{1}{2}\sum_{\alpha=x,y,z} u_\alpha \xi_\alpha(P), \tag{C5}$$

where $u_{x,y} = u_\perp = g_\perp/(2\pi l_B^2)$, $u_z = g_z/(2\pi l_B^2)$, and $\xi_\alpha(P) = {\rm Tr}[\tau_\alpha P]\,{\rm Tr}[\tau_\alpha P] - {\rm Tr}[\tau_\alpha P \tau_\alpha P]$. $\mathcal{E}_{\rm v}(\nabla P)$ is a gradient term, and has a similar expression as $\mathcal{E}_{\rm v}(P)$. The last term is the Zeeman energy

$$\mathcal{E}_{\rm Z}(P) = -\epsilon_{\rm Z}\,{\rm Tr}[\sigma_z P]. \tag{C6}$$

The position-dependent density matrix P has the following properties:

$$P^\dagger = P, \quad {\rm Tr}P = 2, \quad P^2 = P. \tag{C7}$$

It is convenient to reparametrize the state with a matrix R, where $P = \frac{1}{2}(1+R)$. R is Hermitian, traceless, and $R^2 = 1$. Thus, R can be expressed in terms of SU(4) generators:

$$R = \sum_a l_a \gamma_a + \sum_{a>b} l_{ab}\gamma_{ab}, \tag{C8}$$

where l_a and l_{ab} are classical real fields. The condition $R^2 = 1$ gives rise to constraints on these fields. One type is the normalization constraint enforcing ${\rm Tr}[R^2] = 4$:

$$\sum_a l_a^2 + \sum_{a>b} l_{ab}^2 = 1. \tag{C9}$$

Another type are the orthogonality constraints:

$$\epsilon^{abcde} l_{cd} l_e = 0, \quad \epsilon^{abcde} l_{bc} l_{de} = 0, \tag{C10}$$

where ϵ^{abcde} is the fully antisymmetric Levi-Civita symbol in five dimensions. The orthogonality constraint is given by ${\rm Tr}[R^2\gamma_{ab}] = 0$ and ${\rm Tr}[R^2\gamma_a] = 0$.

The SO(5) theory of high-T_c superconductivity [21] requires a similar orthogonality constraint, which plays an essential role in predicting the phase transition between AF and dSC phases. There, it was proposed based on a geometric interpretation of rotations in 5D [21], and separately based on maximum entropy [49] considerations. In our theory, the orthogonality constraint naturally appears because of the assumption that at each LL orbital two spinors are occupied, i.e., that charge fluctuations are quenched. To make the physical meaning of the fifteen fields $\{l_a, l_{ab}\}$ transparent, we rename them using the spin and valley language:

$$\begin{aligned} &l_{34,42,23} = s_{x,y,z}, \quad l_{1,5} = t_{x,y}, \quad l_{15} = t_z, \\ &l_{2,3,4} = n_{x,y,z}, \\ &l_{52,53,54} = \pi^x_{x,y,z}, \quad l_{21,31,41} = \pi^y_{x,y,z}. \end{aligned} \tag{C11}$$

s_α, t_α, and n_α with $\alpha = x,y,z$ are respectively the spin, valley and Néel fields, and there are six π fields. The explicit form of the energy density $\mathcal{H}$ expressed in terms of these classical fields is given in Eq. (6) of the main text.

APPENDIX D: COLLECTIVE MODES IN THE PRESENCE OF A ZEEMAN FIELD

In the presence of Zeeman field, the AF is transformed to a canted antiferromagnetic (CAF) state in which the spin polarizations on opposite sublattices are not collinear. In the CAF state, the density matrix is $P({\rm CAF}) = \frac{1}{2}(1 + \sin\theta_s \tau_z\sigma_x + \cos\theta_s\sigma_z)$, where the canting angle is $\cos\theta_s = \epsilon_{\rm Z}/|2u_\perp|$ [20]. One of the spin wave mode remains gapless in the CAF state:

$$\omega_1({\rm CAF}) = 2\sqrt{\rho_n(2|u_\perp|\sin^2\theta_s + (\rho_n\cos^2\theta_s + \rho_s\sin^2\theta_s)k^2)}k. \tag{D1}$$

This gapless mode corresponds to the rotation of Néel vector within the xy plane. Another spin wave mode acquires a gap:

$$\omega_2({\rm CAF}) = 2\sqrt{(\epsilon_{\rm Z}\cos\theta_s + (\rho_n\sin^2\theta_s + \rho_s\cos^2\theta_s)k^2)(2|u_\perp| + \rho_s k^2)}. \tag{D2}$$

The Zeeman field also modifies the dispersion of the sublattice/π modes:

$$\omega_{3,4}({\rm CAF}) = 2\sqrt{(u_z + u_\perp + \epsilon_{\rm Z}\cos\theta_s + (\rho_\perp\sin^2\theta_s + \rho_\pi\cos^2\theta_s)k^2)(u_z - u_\perp + \rho_\pi k^2)}, \tag{D3}$$

which remain gapped in the CAF phase and become gapless at the CAF/KD phase boundary $u_z + u_\perp + \epsilon_{\rm Z}\cos\theta_s = 0$ [20].

At the SO(5) point $u_z + u_\perp = 0$, the gapped spin wave mode $\omega_2({\rm CAF})$ and sublattice/π modes $\omega_{3,4}({\rm CAF})$ become degenerate. The degeneracy is due to the unbroken part of the SO(5) symmetry in the presence of Zeeman field.

[1] Y. Zhang, Z. Jiang, J. P. Small, M. S. Purewal, Y.-W. Tan, M. Fazlollahi, J. D. Chudow, J. A. Jaszczak, H. L. Stormer, and P. Kim, Phys. Rev. Lett. **96**, 136806 (2006).

[2] A. F. Young, C. R. Dean, L. Wang, H. Ren, P. Cadden-Zimansky, K. Watanabe, T. Taniguchi, J. Hone, K. L. Shepard, and P. Kim, Nat. Phys. **8**, 550 (2012).

[3] X. Du, I. Skachko, F. Duerr, A. Luican, and E. Y. Andrei, Nature (London) **462**, 192 (2009).

[4] K. I. Bolotin, F. Ghahari, M. D. Shulman, H. L. Stormer, and P. Kim, Nature (London) **462**, 196 (2009).

[5] C. R. Dean, A. F. Young, P. Cadden-Zimansky, L. Wang, H. Ren, K. Watanabe, T. Taniguchi, P. Kim, J. Hone, and K. L. Shepard, Nat. Phys. **7**, 693 (2011).

[6] K. Nomura and A. H. MacDonald, Phys. Rev. Lett. **96**, 256602 (2006).

[7] K. Yang, S. Das Sarma, and A. H. MacDonald, Phys. Rev. B **74**, 075423 (2006).

[8] B. E. Feldman, B. Krauss, J. H. Smet, and A. Yacoby, Science **337**, 1196 (2012).

[9] B. E. Feldman, A. J. Levin, B. Krauss, D. A. Abanin, B. I. Halperin, J. H. Smet, and A. Yacoby, Phys. Rev. Lett. **111**, 076802 (2013).
[10] A. F. Young, J. D. Sanchez-Yamagishi, B. Hunt, S. H. Choi, K. Watanabe, T. Taniguchi, R. C. Ashoori, and P. Jarillo-Herrero, Nature (London) **505**, 528 (2014).
[11] D. A. Abanin, B. E. Feldman, A. Yacoby, and B. I. Halperin, Phys. Rev. B **88**, 115407 (2013).
[12] I. Sodemann and A. H. MacDonald, Phys. Rev. Lett. **112**, 126804 (2014).
[13] D. M. Basko and I. L. Aleiner, Phys. Rev. B **77**, 041409(R) (2008).
[14] J. Alicea and M. P. A. Fisher, Phys. Rev. B **74**, 075422 (2006).
[15] I. F. Herbut, Phys. Rev. Lett. **97**, 146401 (2006).
[16] J.-N. Fuchs and P. Lederer, Phys. Rev. Lett. **98**, 016803 (2007).
[17] J. Jung and A. H. MacDonald, Phys. Rev. B **80**, 235417 (2009).
[18] K. Nomura, S. Ryu, and D.-H. Lee, Phys. Rev. Lett. **103**, 216801 (2009).
[19] C.-Y. Hou, C. Chamon, and C. Mudry, Phys. Rev. B **81**, 075427 (2010).
[20] M. Kharitonov, Phys. Rev. B **85**, 155439 (2012).
[21] E. Demler, W. Hanke, and S.-C. Zhang, Rev. Mod. Phys. **76**, 909 (2004).
[22] I. L. Aleiner, D. E. Kharzeev, and A. M. Tsvelik, Phys. Rev. B **76**, 195415 (2007).
[23] S. Ryu, C. Mudry, C.-Y. Hou, and C. Chamon, Phys. Rev. B **80**, 205319 (2009).
[24] I. F. Herbut, Phys. Rev. B **85**, 085304 (2012).
[25] M. Kharitonov, Phys. Rev. B **86**, 075450 (2012).
[26] M. Kharitonov, Phys. Rev. Lett. **109**, 046803 (2012).
[27] M. Kharitonov, Phys. Rev. B **86**, 195435 (2012).
[28] M. Hamermesh, *Group Theory and Its Application to Physical Problems* (Dover, New York, 1989), Chap. 8.
[29] K. Moon, H. Mori, K. Yang, S. M. Girvin, A. H. MacDonald, L. Zheng, D. Yoshioka, and S.-C. Zhang, Phys. Rev. B **51**, 5138 (1995).
[30] A. A. Burkov and A. H. MacDonald, Phys. Rev. B **66**, 115320 (2002).
[31] D. P. Arovas, A. Karlhede, and D. Lilliehook, Phys. Rev. B **59**, 13147 (1999).
[32] L. E. Hayward, D. G. Hawthorn, R. G. Melko, and S. Sachdev, Science **343**, 1336 (2014).
[33] C. Kristjansen, R. Pourhasan, and G. W. Semenoff, J. High Energy Phys. 02 (2014) 097.
[34] R. T. Weitz, M. T. Allen, B. E. Feldman, J. Martin, and A. Yacoby, Science **330**, 812 (2010).
[35] S. Kim, K. Lee, and E. Tutuc, Phys. Rev. Lett. **107**, 016803 (2011).
[36] J. Velasco Jr., L. Jing, W. Bao, Y. Lee, P. Kratz, V. Aji, M. Bockrath, C. N. Lau, C. Varma, R. Stillwell, D. Smirnov, F. Zhang, J. Jung, and A. H. MacDonald, Nat. Nanotechnol. **7**, 156 (2012).
[37] P. Maher, C. R. Dean, A. F. Young, T. Taniguchi, K. Watanabe, K. L. Shepard, J. Hone, and P. Kim, Nat. Phys. **9**, 154 (2013).
[38] S. Rabello, H. Kohno, E. Demler, and S.-C. Zhang, Phys. Rev. Lett. **80**, 3586 (1998).
[39] C. L. Henley, Phys. Rev. Lett. **80**, 3590 (1998).
[40] C. Wu, J.-P. Hu, and S.-C. Zhang, Phys. Rev. Lett. **91**, 186402 (2003).
[41] H.-H. Hung, Y. Wang, and C. Wu, Phys. Rev. B **84**, 054406 (2011).
[42] H. Georgi, *Lie Algebras In Particle Physics: From Isospin To Unified Theories* (Westview Press, Boulder, Colorado, 1999), Chap. 23.
[43] F. D. M. Haldane, Phys. Rev. Lett. **55**, 2095 (1985).
[44] W. Pfeifer, *The Lie Algebras SU(N): An Introduction* (Birkhäuser, Basel, Switzerland, 2003), Chap. 5.
[45] R. Eder, W. Hanke, and S.-C. Zhang, Phys. Rev. B **57**, 13781 (1998).
[46] E. Lieb, T. Schultz, and D. Mattis, Ann. Phys. (NY) **16**, 407 (1961).
[47] B. Bernu, C. Lhuillier, and L. Pierre, Phys. Rev. Lett. **69**, 2590 (1992).
[48] M. Gross, E. Sánchez-Velasco, and E. Siggia, Phys. Rev. B **39**, 2484 (1989).
[49] F. J. Wegner, Eur. Phys. J. B **14**, 11 (2000).